# Discussion of the dynamic stability of a multi-degree-of-freedom rotor system affected by a transverse crack

Roberto Ricci, Paolo Pennacchi[1]
Department of Mechanical Engineering
Politecnico di Milano
Via La Masa 1, 20156 Milan, Italy

**Abstract.** The dynamic behaviour of cracked rotors is one of the most discussed topics in the rotordynamic literature due to the wide range of problems that may arise from this fault. Among them, it is a common notion that cracks in horizontal rotating shafts may cause instability of the system because of the periodic opening and closing of the crack, i.e., the *breathing mechanism*, determines the stiffness variation and the parametric excitation of the rotor system. Simplified models have been used to study this phenomenon using Jeffcott rotors. For the first time in this paper, a model of a real hyperstatic rotor with several degrees of freedom is used, which also considers the bearings and the foundation of the system, and the stability is discussed by means of the Floquet theory. The sensitivity of the obtained results to the system anisotropy and the crack position is also investigated. The results presented are quite different from those obtained by means of the simple Jeffcott rotor but are consistent with real and documented field experiences.
*Keywords: crack, rotordynamics, stability, Floquet theory, multi-dimensional Floquet analysis*

## 1. Introduction

The shafts in rotating machinery used in industrial plants are subjected to heavy working conditions that also include thermal transients. In spite of proper design and accurate manufacturing, the rotor shafts may be affected by fatigue cracks [1]. These cracks generally originate from manufacturing flaws, but their growth is associated with cyclic loading. Because these cracks may lead to catastrophic failures [2], their early detection is desirable.

During rotation, a horizontal cracked shaft is characterised by a time-variant stiffness that depends on the position of the transverse crack with respect to gravity; that is, during one revolution, the crack opens and closes under the effect of the shaft weight [1]. This behaviour is known as the *breathing mechanism*, and the breathing associated with the stress distribution around the crack is responsible for the local variation in the shaft flexibility.

Since the 1950s, many different studies have appeared in the literature on the topic of cracked shafts, and a portion of them are related to the stability of the dynamic behaviour of cracked rotors.

One of the first papers on this subject was written by Gasch [3], who considered the dynamics of a cracked Jeffcott (or de Laval) rotor with two degrees of freedom (d.o.f.) and a hinge model for the breathing mechanism. The same author has further expanded this study over the last thirty years [4][5][6]. The dynamic behaviour of the Jeffcott cracked rotor has been investigated with respect to different rotational speeds, positions and depths of crack as well as with different types of rotor bearings. Gasch also proposed the use of *Floquet theory* to analyse the stability of the dynamic response and performed the so-called *Floquet analysis* (FA), which is based on the determination of the *transition matrix* eigenvalues. Gasch's results show unstable zones caused by cracks located at approximately $2/N \cdot \omega$, where $\omega$ is the natural frequency of the system, and $N$ is an integer

[1] Corresponding author: tel. +39.02.2399.8440, fax +39.02.2399.8492, e-mail: paolo.pennacchi@polimi.it

number. The predictions regarding the dynamic behaviour of Jeffcott cracked rotor have been experimentally verified by Muszyńska [7] using a test-rig that was able to accurately reproduce the behaviour of a Jeffcott rotor.

Other authors in the literature have studied the effect of the breathing mechanism on the system stability; for instance, Huang et al. [8] determined the variation of the flexibility coefficients with respect to the shaft orientation (or the relative position of the crack during the revolution of the shaft). Sekhar studied the influence of one or two cracks on the rotor stability [9][10] by considering the real part of the eigenvalues of the linearised equation of motion. Yang et al. [11] focused their interest on the relationship between the chaotic response and the instability of the cracked rotors. Zhu et al. [12] considered the problem of avoiding instability in a cracked rotor supported by active magnetic bearings. Lin et al. [13] studied the effect of environmental variables on the cracked rotor stability. More recently, Chen et al. [14] and Sinou [15] offered further contributions to the discussion of cracked rotor stability.

Although the phenomenon of the opening and closing of the crack has been thoroughly discussed in the literature, up to the present, the stability of cracked rotors has been studied for simple models only. However, the behaviour of real rotors can be quite different from that of the Jeffcott rotor.

In this paper, a steam unit generator, which has developed a deep crack during its operating history [1][16][17] without showing any symptoms of instability during speed transients, is considered. For the first time, the authors show that this observed behaviour is completely contrary to the results predicted by the simple theoretical models based on Jeffcott rotors.

The aim of this study is to evaluate the stability of a rotor for different values of the rotational speed and the depth of crack by also considering the effects of anisotropy. Large calculation resources are necessary for this type of investigation, and this necessity may partially explain why this type of analysis has not been previously performed on a multi-degrees-of-freedom system.

The paper is organised as follows: in the two next sections, the generator model and the crack modelling are introduced. The main issues of Floquet theory related to the system stability are discussed in Section 4. In Section 5, selected algorithms for the transition matrix evaluation are proposed, and suitable modifications are introduced for managing the complexity of the considered system. The last section of the paper is devoted to a discussion of the stability results obtained by means of numerical calculations.

## 2. Rotor model

The majority of the literature on cracked rotors, apart from those related to the crack-breathing phenomenon, analyses the dynamic behaviour of the rotating machines by carrying out numerical simulations using a Jeffcott rotor with a crack in the disk position.

In these cases, the analytical models and the numerical simulations have shown that the system may become unstable for certain values of the rotational speed and of the crack depth. However, the Jeffcott model, which is useful for the introduction of basic problems, may be not representative of the actual system dynamics (cracked or un-cracked cases), especially in the case of strongly nonlinear systems.

To evaluate the response of actual systems when a crack appears and propagates, the implementation of a more complex model is required.

Among the parts that compose rotating machineries employed in power plants, generators are often affected by cracks. Several such cases in the last 50 years have been documented in [18][19][20][21]. Therefore, the theoretical stability of the dynamic behaviour of a generator,

similar to that described in [1][16][17], is considered in this paper. In these cases, the cracked section reached ~50% of the cross-sectional area (figure 1) when the unit had operated for approximately 133,000 hours. The crack growth proceeded over a period of seven years and approximately 150 start-ups, while only one year was sufficient for the growth of the last 25% of the cross-section area. This generator experienced notably high vibration levels, especially during the last few coast-downs before removal from service; however, the equipment did not display instability.

**Figure 1. Crack shape on the cross-section of a generator (from [1]).**

The portion of the complete machine taken into consideration in this work has length of 17 m and includes the exciter. The external diameters change depending on the position along the rotation axis, the internal diameter remains constant due to the hollow that exists to reduce the rotor weight and to allow the fitting of copper bars. The generator and the exciter are supported by three journal bearings; the first is located near the rigid coupling that connects the generator to the low-pressure turbine, and the others are located at the opposite rotor end.

As shown in figure 2, the model of the rotor is composed of 33 beam elements, and the bearings and pedestals are numbered from left to right. Each finite element has eight d.o.f.s (see figure 3); four of them are the displacements in the two directions orthogonal to the rotating axis, and the other four are the rotations around previous directions. The possible cracked elements that will be considered in the paper are shown as shaded in figure 2, and their positions correspond to those of cracks discovered on real generators (see [1]).

The effect of the oil-film forces in the journal bearings is modelled by means of linearised dynamic coefficients, and the foundation is modelled by means of pedestals.

All of the data shown in figure 4 and figure 5 are provided by the machine manufacturer for rotational speeds ranging from 300 rpm and 3000 rpm and were not recalculated in this work. Note that the pedestal coefficients for supports #1 and #2 are considered as speed-dependent and are tuned to reproduce the horizontal foundation resonance that occurred in the actual machine.

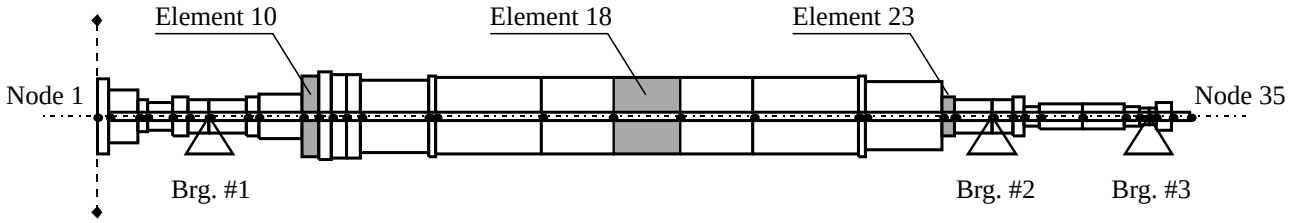


**Figure 2. Finite element model of the generator.**

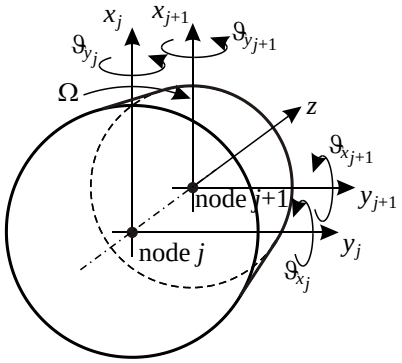


**Figure 3. Beam element with eight d.o.f.s used for rotor modelling.**

Different configurations were tested in terms of modelling to analyse the effects of the bearings and the pedestals on the stability. The four configuration tested are listed in table 1.

**Table 1. Modelling configurations.**

| | *Bearing coefficients* | *Pedestal coefficients* |
|---|---|---|
| Configuration 1 | Constant | Constant |
| Configuration 2 | Dependent on rotational speed | Constant |
| Configuration 3 | Constant | Dependent on rotational speed |
| Configuration 4 | Dependent on rotational speed | Dependent on rotational speed |

In the first configuration, the dynamic coefficients of the bearings and the pedestals are considered to be independent of the rotational speed. Therefore, the stiffness and damping parameters are constant and are equal to the values assumed at 300 rpm.

In the second configuration, the effect of the bearings on the stability has been investigated; the bearing dynamic coefficients vary as shown in figure 4, whereas the foundation values are equal to those of configuration 1.

*Bearing #1*

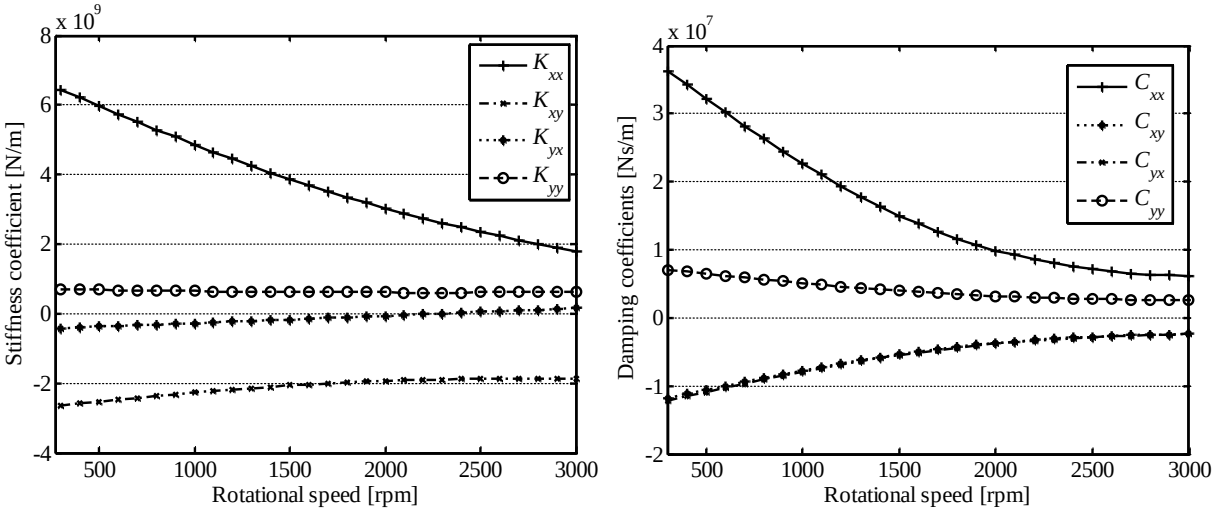


*Bearing #2*

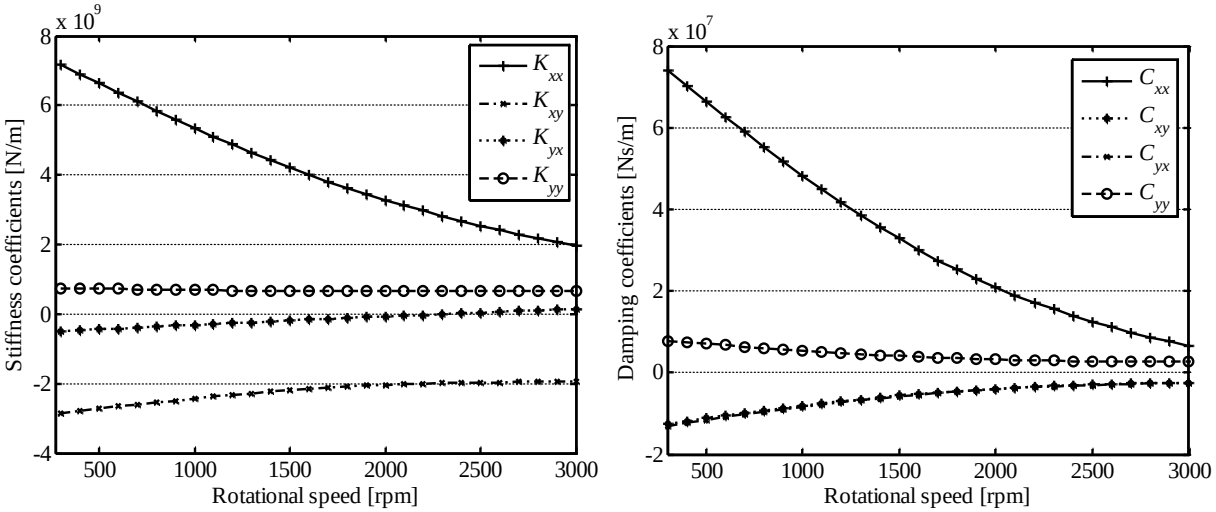


*Bearing #3*

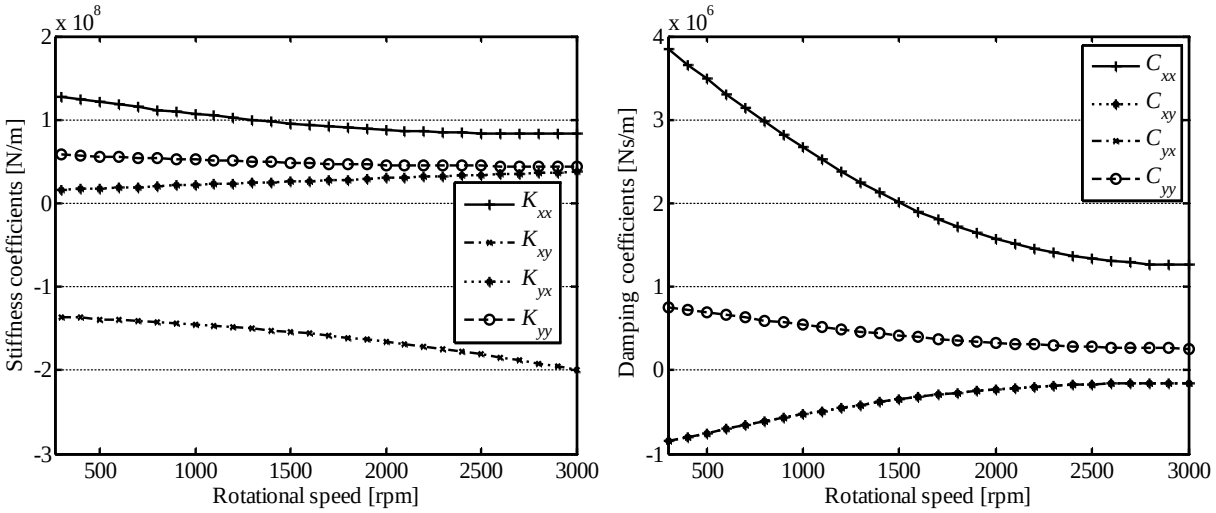


**Figure 4. Linearised stiffness and damping coefficients for the bearings of the generator model.**

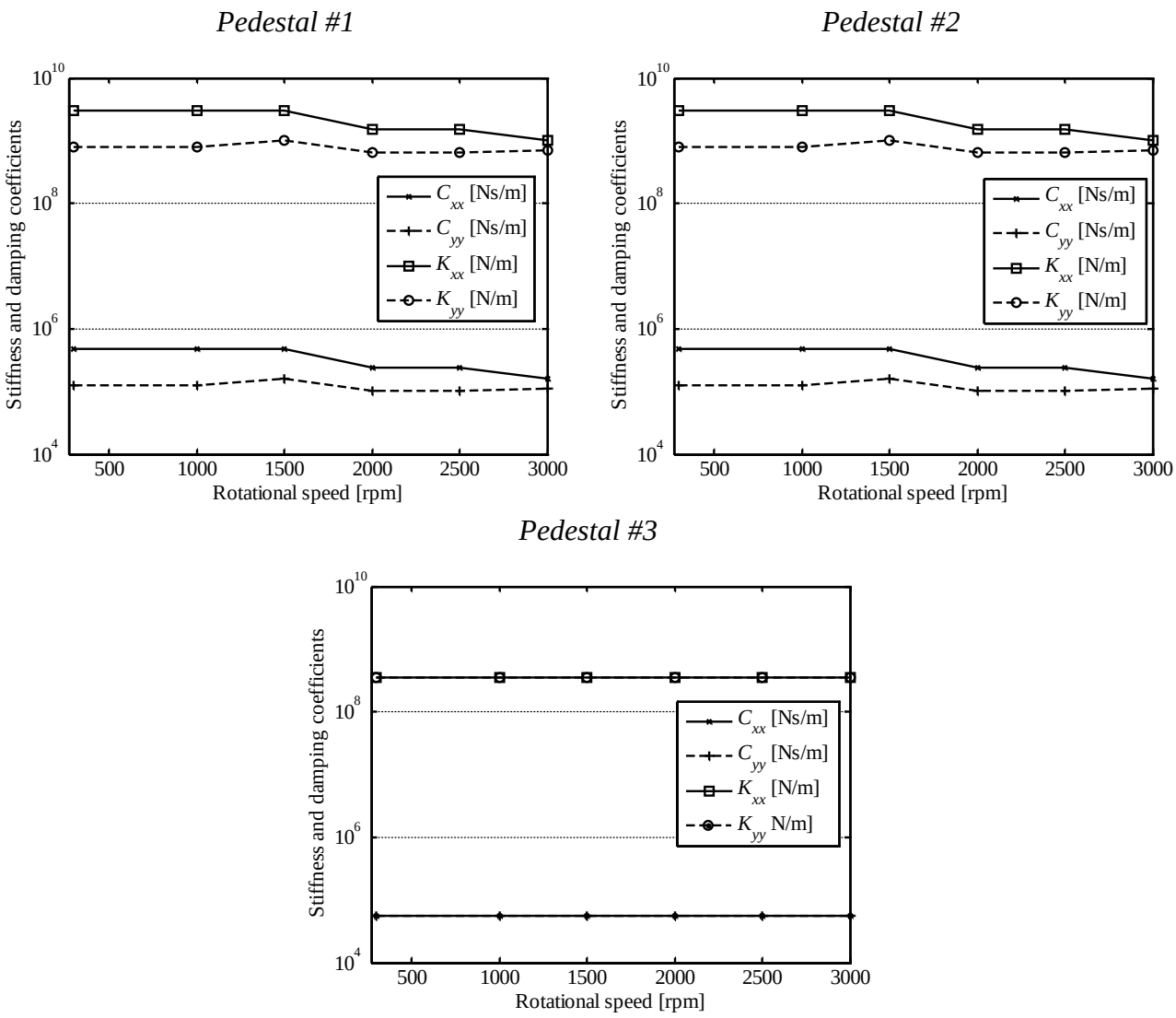


**Figure 5. Linearised stiffness and damping coefficients for the pedestals of the generator model.**

In the third configuration, the effect of the foundation alone is investigated; the stiffness and damping coefficients of the pedestals are defined according to figure 5, while the bearing dynamic coefficients are equal to those of configuration 1.

Finally, in the last configuration, both the bearing and pedestal dynamic coefficients are considered to be speed-dependent, as shown in figure 4 and figure 5.

The matrices of the assembled rotor model (i.e., rotor + bearings + pedestals) are evaluated using RAFT, the software for rotordynamic analysis created by Politecnico di Milano. The mass, the damping, the stiffness and the gyroscopic-effect matrices are calculated for the rotational speed range of 300 rpm to 3000 rpm using steps of 50 rpm. Because four different configurations of the bearing and pedestal models have been considered, the global matrices of the system have been calculated for each configuration.

The simulated response of the rotor system for bearing #1 is shown in figure 6, arising from an unbalance of 0.4 kgm located in the middle of the generator for the four configurations.

It is possible to note that responses are similar in the low rotational speed range because the first critical speeds are practically the same for all configurations and are equal to approximately 720 and 900 rpm, respectively, for the horizontal and vertical directions. In contrast, the second critical

speeds depend on the modelling configuration and range from 2400 to 2600 rpm. Anti-resonance is also present in the horizontal direction close to 2900 rpm for configurations 3 and 4 as a consequence of the foundation resonance.

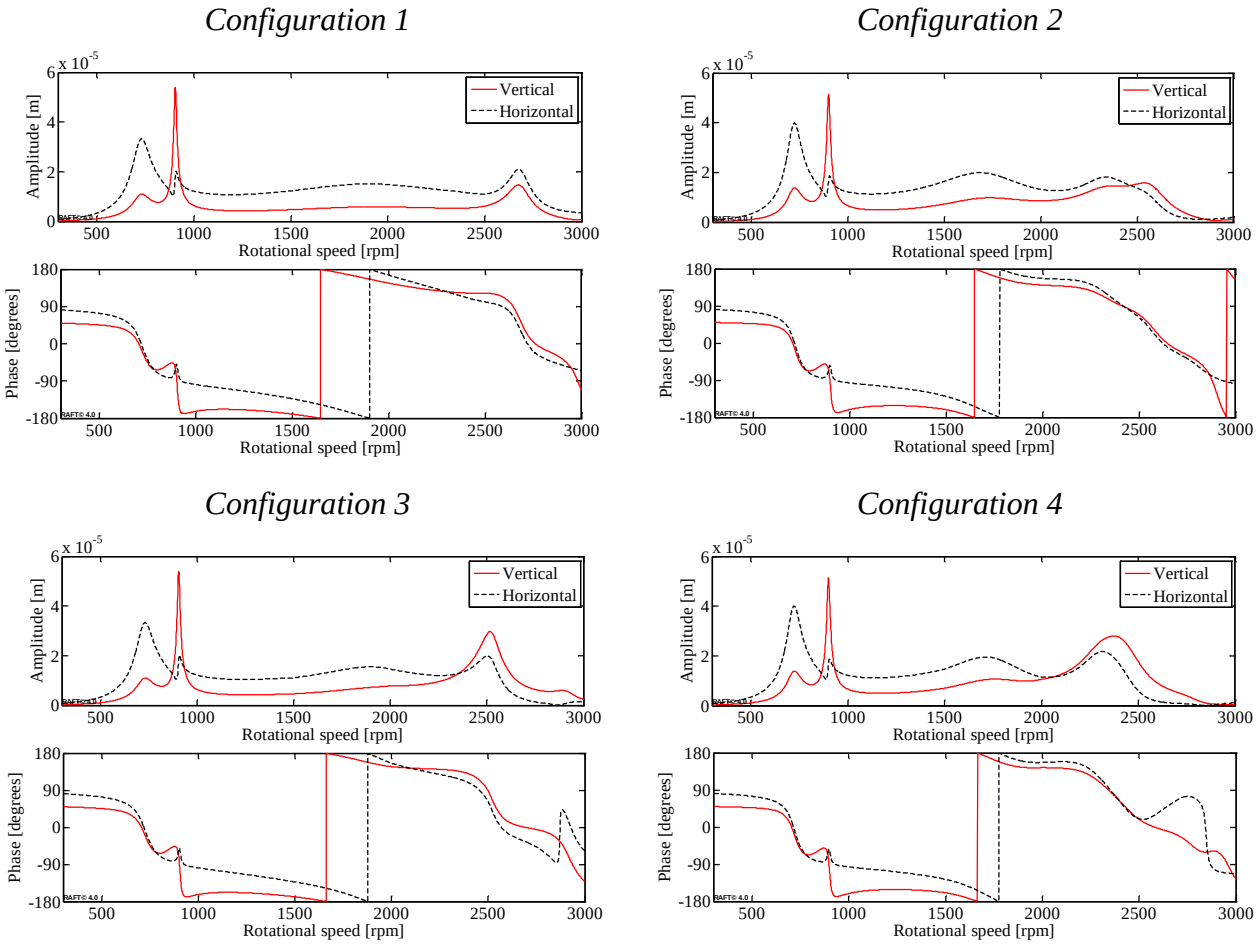


**Figure 6. Unbalance responses of different generator model configurations in bearing #1.**

## 3. Crack modelling

The main consequence of a crack in a rotating shaft is the periodic local variation of the stiffness. Many papers in the literature describe this topic and also consider the second-order effects. In this paper, the rotor stability is related to the periodic variation of the local stiffness created by the presence of a crack by means of periodic variation in the rotor stiffness coefficients. Thus, the system of the motion equations of the horizontal rotor is in the form:

$$\mathbf{M}\ddot{\mathbf{x}} + \mathbf{C}\dot{\mathbf{x}} + \mathbf{K}(\mathbf{x},t)\mathbf{x} = \mathbf{W} + \mathbf{U} \tag{1}$$

where the external force system on the right hand side of Eq. (1) is composed of the weight $\mathbf{W}$ and the unbalance forces $\mathbf{U}$. If a heavy horizontal rotor undamaged by crack is considered, the static deflection $\mathbf{x}_0$ is due to the rotor weight and is largely compared to the additional deflections caused by the dynamics of the rotating shaft [1].

By considering that the stiffness depends on the steering function $\psi(t)$ that governs the breathing mechanism, $\mathbf{K}(\mathbf{x},t)$ can be split into two parts, as shown in [6]:

$$\mathbf{K}(\mathbf{x},t) = \mathbf{K}\left(\mathbf{x},\psi(t)\right) = \mathbf{K}_0 + \Delta\mathbf{K}\left(\mathbf{x},\psi(t)\right) = \mathbf{K}_0 + \Delta\mathbf{K}(\mathbf{x},t) \tag{2}$$

We highlight the weight dominance in Eq. (1) to linearise the equation of motion, by including first Eq. (2) :

$$\mathbf{M}\ddot{\mathbf{x}} + \mathbf{C}\dot{\mathbf{x}} + \left(\mathbf{K}_0 + \Delta\mathbf{K}(\mathbf{x},t)\right)\mathbf{x} = \mathbf{W} + \mathbf{U} \tag{3}$$

and then the rotor deflections are split into the static $\mathbf{x}_0$ and the dynamic parts $\Delta\mathbf{x}(t)$:

$$\mathbf{x}(t) = \mathbf{x}_0 + \Delta\mathbf{x}(t) \tag{4}$$

with $\Delta\mathbf{x}(t)$ $\mathbf{x}_0$. Therefore, Eq. (3) becomes:

$$\mathbf{M}\Delta\ddot{\mathbf{x}} + \mathbf{C}\Delta\dot{\mathbf{x}} + \left(\mathbf{K}_0 + \Delta\mathbf{K}(\mathbf{x}_0 + \Delta\mathbf{x}(t),t)\right)\left(\mathbf{x}_0 + \Delta\mathbf{x}\right) = \mathbf{W} + \mathbf{U} \tag{5}$$

For the static equilibrium:

$$\mathbf{K}_0\mathbf{x}_0 = \mathbf{W} \tag{6}$$

The weight deflection is dominant and will govern the opening and closing of the crack because the vibration amplitudes $\Delta\mathbf{x}(t)$ are small compared to the static deflection $\mathbf{x}_0$ ; then, $\Delta\mathbf{K}(\mathbf{x},t) = \Delta\mathbf{K}(t)$. The equations of motion become linear, but periodically time-variant:

$$\mathbf{M}\Delta\ddot{\mathbf{x}} + \mathbf{C}\Delta\dot{\mathbf{x}} + \left(\mathbf{K}_0 + \Delta\mathbf{K}(t)\right)\Delta\mathbf{x} = -\Delta\mathbf{K}(t)\mathbf{x}_0 + \mathbf{U} \tag{7}$$

because the static equilibrium can be separated.

The periodic time-variant stiffness matrix $\Delta\mathbf{K}(t)$ appears twice. On the left-hand side, it determines whether the system is stable (together with the damping). The homogenous part of Eq. (7) contains periodically time-variant coefficients, and its stability can be evaluated by means of the Floquet theory.

The relationship between the stiffness variation of the cracked elements and the crack depth for the generator considered in Section 2 (as shown in figure 7) has been evaluated by considering a 3D FEM model of the parts in which the crack develops at different depths (see figure 8).

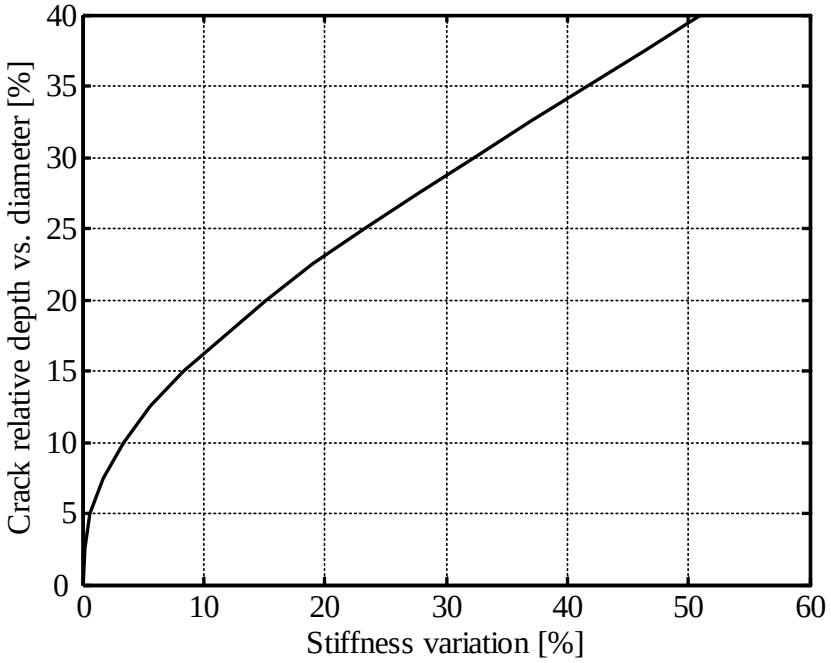


**Figure 7. Stiffness variation as a function of crack depth.**

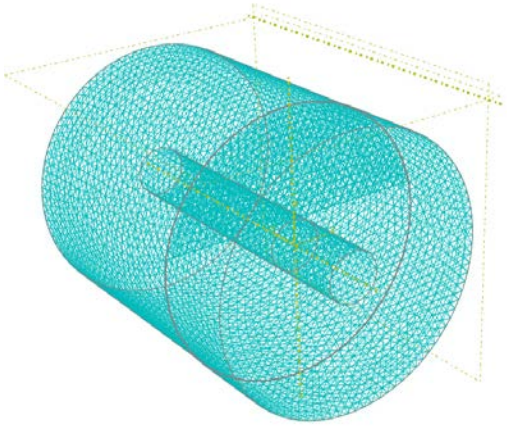

**Figure 8. 3D FEM model used to calculate the stiffness variation as a function of crack depth of figure 7.**

The selection of the most suitable steering function $\psi(t)$ depends on the crack breathing mechanism. In the past, modelling of the breathing has been usually disregarded in the stability analysis, and the transition from a closed crack to an open crack has been generally considered to be abrupt [3], as in the so called *hinge model*, or given by a trigonometric function [22]. Gasch states in [6] that the breathing function can be expressed by means of a switching function for a small depth of crack, while a more complex expression (i.e., a cosine Fourier expansion) is advisable for deeper cracks.

This observation can be explained not only by the need for simplification but also by the fact that the strain energy release rate (SERR) approach (discussed by Papadopuolos [23] and often used in solid mechanics to calculate the additional flexibility caused by a crack) is valid only for the fully open crack. The SERR approach cannot be extended to other intermediate situations that are typical of rotating shafts without the application of rather complex modifications to the SERR approach, as shown by Darpe et al. [24] and Papadoupolos [25]. The same approach also has been used by Xu et al. [26] for time-step calculations in which the breathing behaviour was also determined by the vibrations. Varé and Andrieux [27] developed a model in the time domain in which the true breathing mechanism, or the compliance of the cracked element, is directly evaluated by means of a 3D model as a function of the applied forces in each time step. In addition, Georgantzinos and Anifantis [28] used the finite element approach for modelling the breathing phenomenon. They considered different configurations and the depth and shape of the crack, and performed a non-linear analysis to take into account the contacts that occur between the crack surfaces when the crack closes. The variation in the stiffness coefficients that was obtained is quite similar to the trends proposed in other studies.

A simplified approach that is also able to take into account the presence of thermal transients is presented by Bachschmid et al. [29] and validated by experimental tests performed on a crack specimen [30]. These last tests showed that the steering function is dissimilar to the on-off function, but a transition phase exists between the closed and open crack configuration. Therefore, the steering function used in this paper (shown in figure 9) is obtained from the experimental tests described in [1][30].

## 4. Application of the Floquet theory to the multi-degrees of freedom rotor system

To better understand the results obtained in the next sections, we review the basics of the multi-dimensional Floquet theory. The equations of the free motion of a general mechanical system with $m$ d.o.f.s are usually described in matrix form as:

$$\mathbf{M}\ddot{\mathbf{x}}(t)+\mathbf{C}\dot{\mathbf{x}}(t)+\mathbf{K}\mathbf{x}(t)=\mathbf{0} \tag{8}$$

where $\mathbf{M}$, $\mathbf{C}$, and $\mathbf{K}$ are the mass, damping, and stiffness system matrices, respectively, and $\mathbf{x}(t)$ is the vector of the generalised displacements. Because free motion is considered, the right-hand side of the second-order differential matrix equation is set equal to zero.

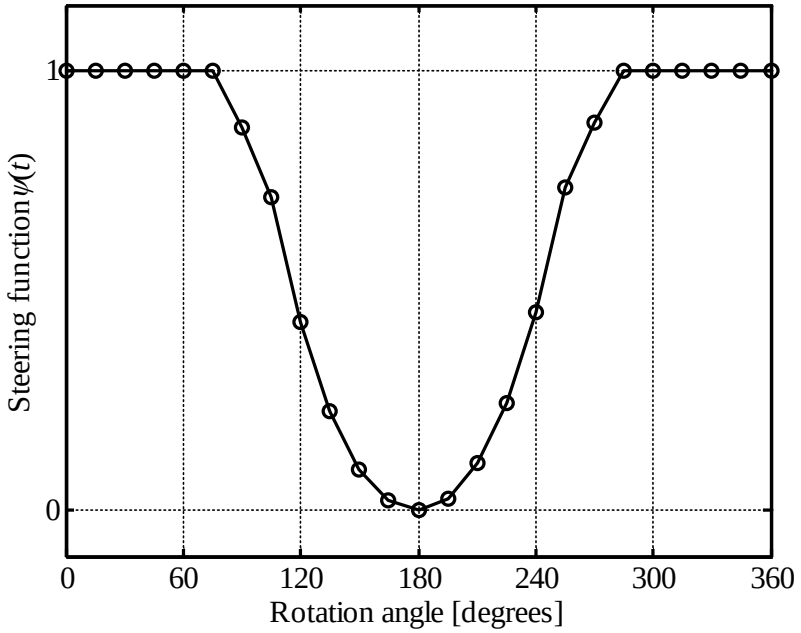


**Figure 9. Steering functions used for modelling the crack breathing mechanism.**

The free motion of the mechanical system can also be described in terms of the state equation. An identity is added to Eq. (2) such that:

$$\begin{aligned}\mathbf{M}\ddot{\mathbf{x}}(t)+\mathbf{C}\dot{\mathbf{x}}(t)+\mathbf{K}\mathbf{x}(t)&=\mathbf{0}\\ \mathbf{M}\dot{\mathbf{x}}(t)&=\mathbf{M}\dot{\mathbf{x}}(t)\end{aligned} \tag{9}$$

and a change of variables is performed:

$$\mathbf{y}(t)=\begin{Bmatrix}\dot{\mathbf{x}}(t)\\ \mathbf{x}(t)\end{Bmatrix};\ \dot{\mathbf{y}}(t)=\begin{Bmatrix}\ddot{\mathbf{x}}(t)\\ \dot{\mathbf{x}}(t)\end{Bmatrix} \tag{10}$$

By substituting the new variables of Eq. (4) into Eq. (3), we obtain:

$$\begin{bmatrix}\mathbf{M} & \mathbf{0}\\ \mathbf{0} & \mathbf{M}\end{bmatrix}\dot{\mathbf{y}}(t)+\begin{bmatrix}\mathbf{C} & \mathbf{K}\\ -\mathbf{M} & \mathbf{0}\end{bmatrix}\mathbf{y}(t)=\mathbf{0} \tag{11}$$

It is now possible to define the matrices $\mathbf{B}$ and $\mathbf{D}$, of size $(2m\times 2m)=(n\times n)$, as:

$$\mathbf{B}=\begin{bmatrix}\mathbf{M} & \mathbf{0}\\ \mathbf{0} & \mathbf{M}\end{bmatrix},\qquad \mathbf{D}=\begin{bmatrix}\mathbf{C} & \mathbf{K}\\ -\mathbf{K} & \mathbf{0}\end{bmatrix} \tag{12}$$

Next, the system of the two matrix equations in Eq. (5) becomes:

$$\mathbf{B}\dot{\mathbf{y}}(t)+\mathbf{D}\mathbf{y}(t)=\mathbf{0} \tag{13}$$

where matrix $\mathbf{B}$ is symmetric and positive because it is composed of the system mass matrices. By imposing:

$$\mathbf{A}=-\mathbf{B}^{-1}\mathbf{D} \tag{14}$$

the system becomes:

$$\dot{\mathbf{y}}(t)=\mathbf{A}\mathbf{y}(t) \tag{15}$$

The square matrix $\mathbf{A}$ is the *state matrix* of the system because it represents the connection between the vector of the variables and their derivatives. If the physical characteristics of the mechanical system are time-dependent, i.e., change with the time $t$, then Eq. (9) is rewritten as:

$$\dot{\mathbf{y}}(t)=\mathbf{A}(t)\mathbf{y}(t) \tag{16}$$

The shaft stiffness changes periodically due to the breathing effect for rotating systems affected by a crack whose equation of motion is given by Eq. (7). In this case, by using $T$ to indicate the period of the rotating system, it is possible to consider the state matrix as periodic:

$$\mathbf{A}(t)=\mathbf{A}(t+T) \tag{17}$$

The Floquet theory is suitable for application to systems modelled by means of time-dependent and periodic ordinary differential equations [31][32]. The main steps of the multi-dimensional FA, performed by applying the multi-dimensional Floquet theory, are presented in this work, beginning with the first-order system described in Eq. (10), to better understand both the meaning and the usefulness of Floquet theory in the study of rotating system stability.

The fundamental theorem of the Floquet theory states that the regular system of Eq. (10) has at least one non-trivial solution of the type:

$$\mathbf{y}(t)=\boldsymbol{\chi}(t) \tag{18}$$

such as:

$$\boldsymbol{\chi}(t+T)=\mu\boldsymbol{\chi}(t) \tag{19}$$

With the aim of demonstrating the theorem statement, the *fundamental matrix* of the system is defined as:

$$\boldsymbol{\Phi}=\left[\phi_{ij}(t)\right] \tag{20}$$

The fundamental matrix is the matrix of the solutions of the system in Eq. (10) such that:

$$\dot{\boldsymbol{\Phi}}(t)=\mathbf{A}(t)\boldsymbol{\Phi}(t) \tag{21}$$

Because $\mathbf{A}(t)$ is periodic, $\boldsymbol{\Phi}(t+T)$ also satisfies the same equation:

$$\dot{\boldsymbol{\Phi}}(t+T)=\mathbf{A}(t)\boldsymbol{\Phi}(t+T) \tag{22}$$

Because:

$$\det\left(\boldsymbol{\Phi}(t+T)\right)\neq 0 \tag{23}$$

matrix $\mathbf{\Phi}(t+T)$ is another fundamental matrix, the columns of which represents the solutions of the system and are linear combinations of those of $\mathbf{\Phi}(t)$; the relationship between the two fundamental matrices is:

$$\phi_{ij}(t+T) = \sum_{k=1}^{n} \phi_{ik}(t) \cdot e_{kj} \tag{24}$$

where $e_{kj}$ are constants. This is equivalent in matrix form to:

$$\mathbf{\Phi}(t+T) = \mathbf{\Phi}(t)\mathbf{E} \tag{25}$$

The determinant of $\mathbf{E}$ is different from zero because the determinants of both fundamental matrices are different from zero. The matrix $\mathbf{E}$ is then non-singular and can be calculated as:

$$\mathbf{E} = \mathbf{\Phi}(t)^{-1}\mathbf{\Phi}(t+T) \tag{26}$$

After the definition of this matrix, it is possible to determine the eigenvalues of $\mathbf{E}$ by means of:

$$\det(\mathbf{E} - \mu\mathbf{I}) = 0 \tag{27}$$

where $\mu$ is a generic matrix eigenvalue. The eigenvector $\mathbf{s}$ corresponding to the eigenvalue $\mu$ is:

$$(\mathbf{E} - \mu\mathbf{I})\mathbf{s} = 0 \tag{28}$$

It is now possible to define:

$$\boldsymbol{\chi}(t) = \mathbf{\Phi}(t)\mathbf{s} \tag{29}$$

which is a solution of the system in Eq. (10) because it is a linear combination of the columns of the fundamental matrix $\mathbf{\Phi}(t)$. By evaluating Eq. (23) after a period $T$:

$$\boldsymbol{\chi}(t+T) = \mathbf{\Phi}(t+T)\mathbf{s} \tag{30}$$

and replacing Eq. (19) in Eq. (24), it follows that:

$$\boldsymbol{\chi}(t+T) = \mathbf{\Phi}(t)\mathbf{E}\mathbf{s} = \mathbf{\Phi}(t)\mu\mathbf{s} \tag{31}$$

and by means the relation expressed by Eq. (23), Eq. (25) becomes:

$$\boldsymbol{\chi}(t+T) = \mu\boldsymbol{\chi}(t) \tag{32}$$

which is the statement of the Floquet theorem.

Matrix $\mathbf{E}$ is called the *transition matrix,* and its eigenvalues are known as the *characteristic multipliers*. From a physical point of view, $\mathbf{E}$ represents the evolution of the modelled system during one period; this assumption can be easily understood by considering that $\mathbf{E}$ expresses the relationship between the fundamental matrices at times $t$ and $t+T$. Therefore, the eigenvalues of the matrix $\mathbf{E}$ are indices of the system stability. An unstable system is characterised by expansive motion, i.e., the solution of the equation at time $t+T$ is "larger" than that calculated at time $t$. In contrast, the system is stable when the solutions do not increase at each period. By considering that the relationship between the fundamental matrices after a period $T$ is represented by a linear combination by means of the transition matrix $\mathbf{E}$ (see eq. (19)), the condition for the system stability is:

$$\left|\mu_i\right| < 1 \quad \forall \mu_i \tag{33}$$

Therefore, performing a stability analysis of the modelled system is quite simple by means of FA after the definition of the transition matrix **E** because it is based on its eigenvalues. Unfortunately, the analytical determination of the transition matrix is impossible for rotor systems modelled with several d.o.f.s, and thus numerical approaches must be used.

## 5. Algorithms for the evaluation of the transition matrix

Several different algorithms for FA are proposed in the literature, and two of them are considered in this paper. The first is called the *single-iteration pass* (SIP) and allows the transition matrix to be calculated by means of one integration only (i.e., straight integration). The second algorithm is called the *n-integration passes* (NIP) and, in contrast to the first algorithm, is based on *n* integrations with *n* equal to twice the number of d.o.f.s (i.e., the system size).

The two algorithms are quite different in terms of both implementation and required computational time. Contrary to what is stated in [33], in which the application of FA to simple systems leads to misleading conclusions, the two algorithms may provide different results. The differences in the required computational time and the results will be discussed in the next subsection.

It is worth noting that other methods have also been suggested in the literature for the analysis of periodic systems, namely the *Chebyshev polynomials* ([34], [35]), the *finite time element methods* ([36], [37]), and the so-called *semi-discretisation method* ([37], [38]). Chebyshev polynomials are based on the same algorithms discussed in this work, and the collocation approach is useful when the equation coefficients are characterised by discontinuities. Because the stiffness matrix definition is continuous in time (i.e., the steering function is continuous in time), the collocation approach is not required in this application. The other two methods have been used successfully to study machine tool chatter.

### *5.1. Single-integration pass algorithm*

The most immediate approach uses the SIP algorithm [33], which is based on the definition of the transition matrix between the initial condition and the condition after one period (i.e., $t = 0$ and $t = T$). By considering Eqs. (15), (16) and (20), it follows that:

$$\mathbf{E}\left(0,T\right) = \mathrm{e}^{\mathbf{A}(t)T} \tag{34}$$

This method foresees the approximation of the time-dependent state matrix by means of a series of constant matrices. To obtain this objective, the period $T$ is divided into $K$ equal intervals of amplitude $\Delta$: at each interval $t_k$, with $0 \le k \le K$ and $0 < t_1 < t_2 < \cdots < t_k \cdots < t_K = T$, $\mathbf{A}\left(t\right)$ is evaluated:

$$\mathbf{C}_k = \frac{1}{\Delta}\int_{t_{k-1}}^{t_k} \mathbf{A}\left(\xi\right)\mathrm{d}\xi, \qquad \xi \in \tau_k \tag{35}$$

where $\tau_k = t_k - t_{k-1}$. The transition matrix can be obtained as a product over all of the intervals:

$$\mathbf{E}_a\left(0,T;K\right) = \mathrm{e}^{\Delta_K \mathbf{C}_K}\ \mathrm{e}^{\Delta_{K-1}\mathbf{C}_{K-1}} \cdots \mathrm{e}^{\Delta_1 \mathbf{C}_1} = \prod_{k=1}^{K} \mathrm{e}^{\Delta_k \mathbf{C}_k} \tag{36}$$

where the transition matrix is notated as $\mathbf{E}_a\left(0,T;K\right)$ with subscript *a* indicating that an approximation has been introduced by considering the constant matrices instead of the real matrices. Next, the terms of the product in Eq. (30) can be expressed by exploiting the definition of the matrix exponential as:

$$\mathrm{e}^{\Delta_k \mathbf{C}_k} = \mathbf{I} + \sum_{j=1}^{\infty} \frac{\left(\Delta_k \mathbf{C}_k\right)^j}{j!} \tag{37}$$

For sufficiently small time intervals, the series in the previous equation can be evaluated by means of a finite number of terms:

$$\mathrm{e}^{\Delta_k \mathbf{C}_k} \cong \mathbf{I} + \sum_{j=1}^{J} \frac{\left(\Delta_k \mathbf{C}_k\right)^j}{j!} \tag{38}$$

where the number of terms $J$ is usually taken as equal to 4. The second approximation of the transition matrix calculation is then related to the evaluation of the elements of the product, and the error induced for each element is given by the remainder of the series:

$$\sum_{j=J+1}^{\infty} \frac{\left(\Delta_k \mathbf{C}_k\right)^j}{j!} \tag{39}$$

With these considerations, the transition matrix after two approximations $\mathbf{E}_{aa}$ can be obtained by means of the following expression:

$$\mathbf{E}_{aa}\left(0,T;K\right) = \prod_{i=1}^{K} \left( \mathbf{I} + \sum_{j=1}^{J} \frac{\left(\Delta_k \mathbf{C}_k\right)^j}{j!} \right) \tag{40}$$

The SIP algorithm works correctly in the FA of simple models, but it is affected by numerical problems when more complex and computationally expensive models are considered, i.e., those with “bigger” size. These problems are closely related to the evaluation of the exponential matrix, which is a delicate operation from a numerical point of view.

The calculation of the exponential matrix can be performed in several ways [39], [40], [41]. One way is to use a series expansion, such as the Taylor expansion, and the performances of the algorithms based on this approach depend on the number of terms considered in the expansion. The *a priori* definition of the optimal number of expansion terms to be considered is the critical point of this method ([42], [43]): the accuracy of the calculation of the matrix exponential does not increase proportionally with the increase in the number of the expansion terms considered. This problem is widely known in computational mathematics as the *Hump phenomenon*.

To solve this problem, the authors propose the use of iSIP, which is a modification of the SIP algorithm by means of the use of a Pade approximation for the calculation of the exponential matrix. The Pade approximation [44] is a ratio between two expansions:

$$e^{\mathbf{A}} \approx \mathbf{B} = \frac{\left(a_0\mathbf{I} + a_1\mathbf{A} + a_2\mathbf{A}^2 + \ldots + a_p\mathbf{A}^p\right)}{\left(b_0\mathbf{I} + b_1\mathbf{A} + b_2\mathbf{A}^2 + \ldots + b_q\mathbf{A}^q\right)} \tag{41}$$

The Pade approximation is accurate only for $\left\|\mathbf{A}\right\|_2 < 1/2$, otherwise the *scaling and squaring method* is considered [45]. This method is based on the consideration that:

$$e^{\mathbf{A}} = \left(e^{\mathbf{A}/2}\right)^2 = \left(e^{\mathbf{A}/2^k}\right)^{2^k} \tag{42}$$

If $|\mathbf{A}| > 1/2$ then $|\mathbf{A}|/2^k < 1/2$ for $k < \log_2(|\mathbf{A}|)+1$, the Pade approximation is calculated and then raised to the second power $k$ times. This modification renders the first algorithm suitable for the multi-dimensional FA of complex rotor models.

*5.2. N-integration passes algorithm*

The NIP algorithm is based on the evaluation of the fundamental matrices at both the beginning and the end of the period. The initial fundamental matrix can be expressed as [33]:

$$\mathbf{\Phi}(0) = \left[\mathbf{y}_1(0) \,|\, \mathbf{y}_2(0) \,|\cdots|\, \mathbf{y}_n(0)\right] \tag{43}$$

where the $i\,th$ column vector represents the *activation* of the $i\,th$ d.o.f. of the system and is defined as:

$$\mathbf{y}_i(0) = \begin{Bmatrix} 0 \\ i \\ \vdots \\ 0 \end{Bmatrix} \tag{44}$$

The meaning of the *activation vector* in Eq. (38) is that only the $i\,th$ d.o.f. assumes an initial value different from zero in the $i\,th$ vector, while the others are all null elements. The corresponding vector $\mathbf{y}_i(T)$ at the end of the period $T$ can be obtained by means of numeric integration of the differential system of equations describing the model dynamics. It is worth noting that vector $\mathbf{y}_i(T)$ is generally composed of all non-zero elements because the equations are not uncoupled.

The fundamental matrix at the end of the period is expressed as:

$$\mathbf{\Phi}(T) = \left[\mathbf{y}_1(T) \,|\, \mathbf{y}_2(T) \,|\cdots|\, \mathbf{y}_n(T)\right] \tag{45}$$

where the $\mathbf{y}_i(T)$ column vector represents the vector obtained by means of the numerical integration over the period $T$ with the initial conditions expressed by the $\mathbf{y}_i(0)$ vector.

From a practical point of view, the two fundamental matrices can be evaluated by imposing one d.o.f. at a time different from zero in the initial vector $\mathbf{y}(0)$ and then numerically integrating the equations of motion to obtain the corresponding $\mathbf{y}(T)$. By repeating this procedure for all $n$ d.o.f.s of the system, the definition of the initial and the final fundamental matrices is possible.

The transition matrix, as previously presented in Eq. (20), is given by:

$$\mathbf{E}(T,0) = \mathbf{\Phi}(0)^{-1}\,\mathbf{\Phi}(T) \tag{46}$$

This algorithm is more interesting for full comprehension of the physical meaning of the transition matrix. Indeed, the transition matrix compares the final condition of the system with the initial condition. The initial fundamental matrix can be considered as an *activation matrix* because the $i\,th$ column vector represents the activation of the $i\,th$ d.o.f. only.

However, similar to the SIP algorithm, the NIP is also affected by computational inaccuracies when models with several d.o.f.s are considered. In this case, the increase in the dimension of the

matrices involved in integration by the Runge-Kutta method presents a limitation on the use of NIP. A suitable modification of this algorithm is proposed hereafter by the authors, similar to what was performed for the single iteration pass.

The Runge-Kutta method, which is often employed in the literature regarding FA for the numerical integration of the motion equations, has been replaced with the Newmark method, and the remaining steps are unchanged (from Eq. (37) to Eq. (39)). The Newmark method uses matrices with dimensions consistent with those of Eq. (6), contrary to the Runge-Kutta method. The corresponding NIP modified algorithm is indicated hereafter as NIPN.

### *5.3. Comparison between the different algorithms*

The improved SIP (iSIP) algorithm (i.e., SIP with the Pade approximation and the scaling and squaring method), the NIP, and the NIPN algorithms are used to perform the FA on a cracked Jeffcott rotor model, and the results are compared. The natural frequency of the uncracked Jeffcott rotor is 15 Hz (i.e., 900 rpm), and the damping is equal to 2% of the critical damping.

The results obtained are shown in Figure 10 in which the value of the characteristic multiplier is plotted on the left side, and the contour map of the level equal to 1 is plotted on the right. The collective results are similar and coherent with those from the studies proposed in the past, except for NIPN, in which the use of the Newmark method causes the introduction of additional damping in the system. Instability arises for rotational speeds of approximately 600 rpm, 900 rpm, and 1800 rpm: the first value represents the 2/3 sub-synchronous component of the flexural critical speed while the others are its 1X and 2X harmonics. The positions of the instability zones correspond to those of [1], [3], [4], [5] and [6], except for NIPN, for which the sub-synchronous zone disappears due to the additional damping introduced.

The iSIP will be used to carry out the FA on the generator model presented in Section 2 because the analysis performed by means of the iSIP confirms the results already obtained in literature and because it is the fastest method from a computational point of view when applied to systems with several d.o.f.s.

## 6. Results of the Floquet analysis applied to the generator model

As previously mentioned in Sections 2 and 3, the simulations were performed for four different configurations of the bearings and pedestals and for three different crack positions located along the shaft axis for a total number of twelve simulations. Each simulation was performed for rotational speeds ranging from 300 rpm to 3000 rpm and crack depths in the range of 0–25% of the rotor diameter. Although the rotational speed range has been selected by considering the typical speed transients of the generator, the maximum crack depth has been limited under the following constraints: i) the computational time required by each simulation and ii) the presence of a crack with 25% depth is considered to be too dangerous for operation of the rotor. A single simulation includes 254 rotational speeds and 11 crack depths in the aforementioned ranges for a computational time of approximately five days of PC work. In this way, the transition matrices and the characteristic multipliers are obtained for each configuration at the different rotational speeds and crack depths.

According to Eq. (27), instability arises when at least one characteristic multiplier is greater than one. From a practical point of view, this implies a check of all of the characteristic multipliers calculated from the transition matrix. However, the multipliers can be grouped by considering their magnitudes. Therefore, only one multiplier for each group must be checked, thus avoiding a one-by-one assessment. For this reason and for the sake of brevity, not all exponents will be reported

and discussed in this work. Only two multipliers are shown, namely, the 1st and the 40th, which represent the different categories of magnitude.

*iSIP*

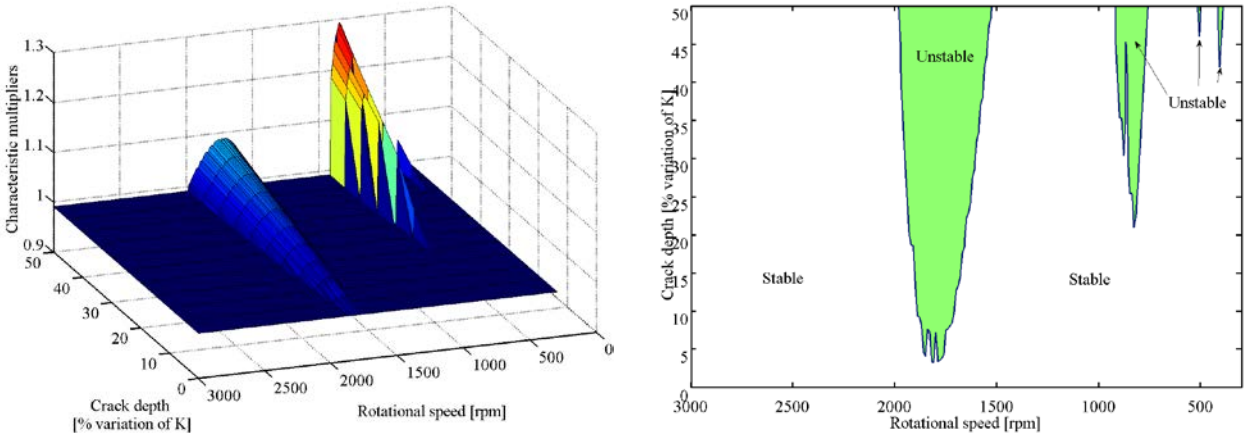


*NIP*

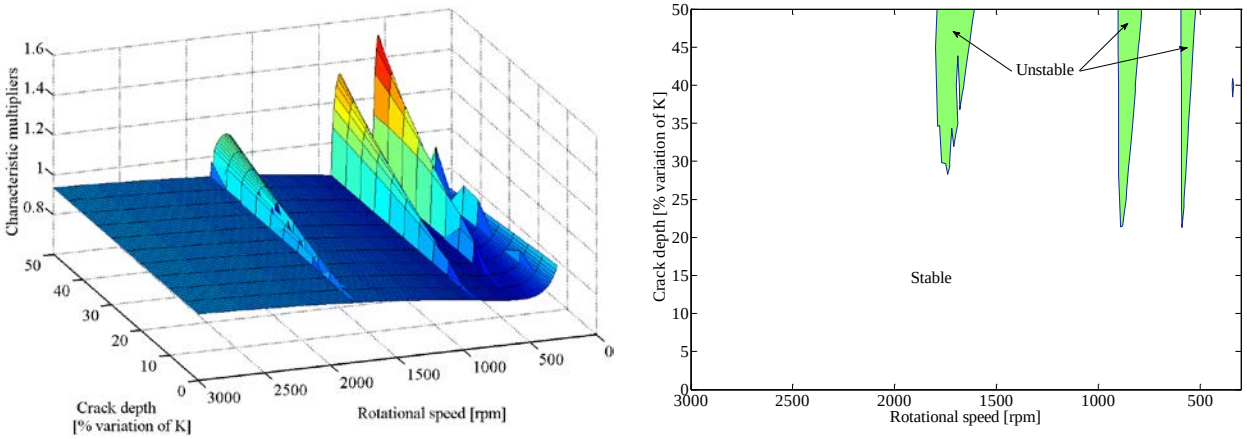


*NIPN*

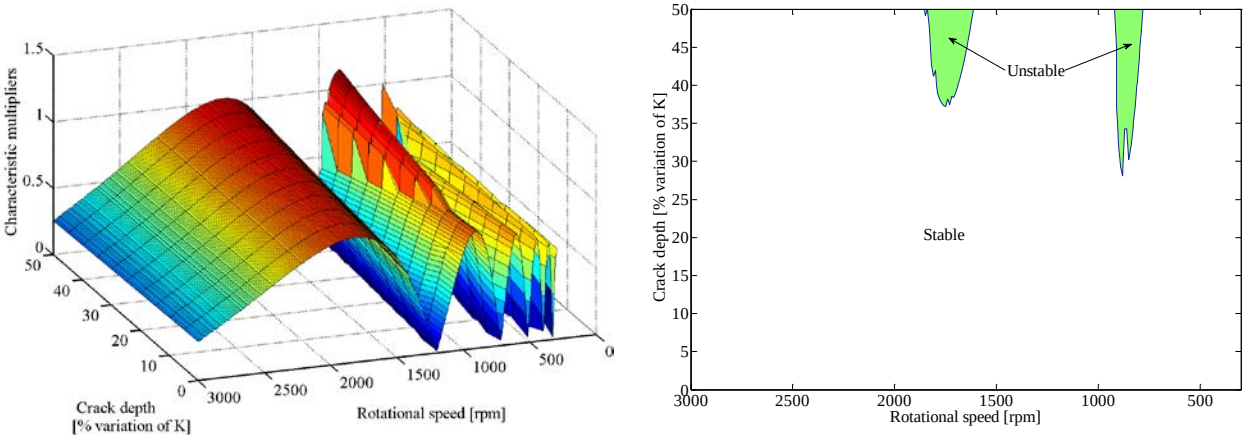


**Figure 10. Characteristic multiplier for a cracked Jeffcott rotor with a natural frequency of 15 Hz.**

Figure 11 shows the distributions of the first characteristic multiplier for a crack in the 10th element for the four configurations. It should be noted that the multiplier distribution is quite

different from that proposed in [1], [3], [4], [5] and [6] for any Jeffcott rotor: the dynamic stability of the generator is guaranteed by the fact that the multiplier is lower than one for all conditions of the rotational speed and crack depth. The trend of the multiplier seems mainly governed by the speed and is practically independent from the crack depth. The values close to one are obtained in correspondence with low rotational speeds while a sort of plateau appears at high speeds. The results are nearly the same for all four configurations. Therefore, the results obtained for the first characteristic multiplier and for a crack in the 10$^{th}$ element of the generator indicate that the system is stable, independent from the rotational speed and crack depth considered. Moreover, the different approaches to modelling of the bearings and foundation have negligible effects on the multiplier distribution and thus on the stability of the generator.

*Configuration 1* *Configuration 2*

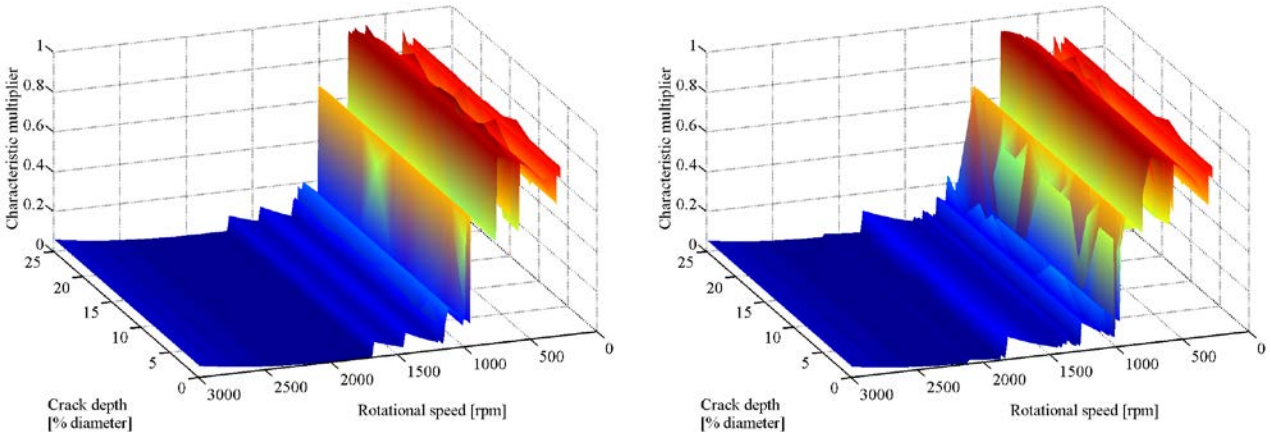


*Configuration 3* *Configuration 4*

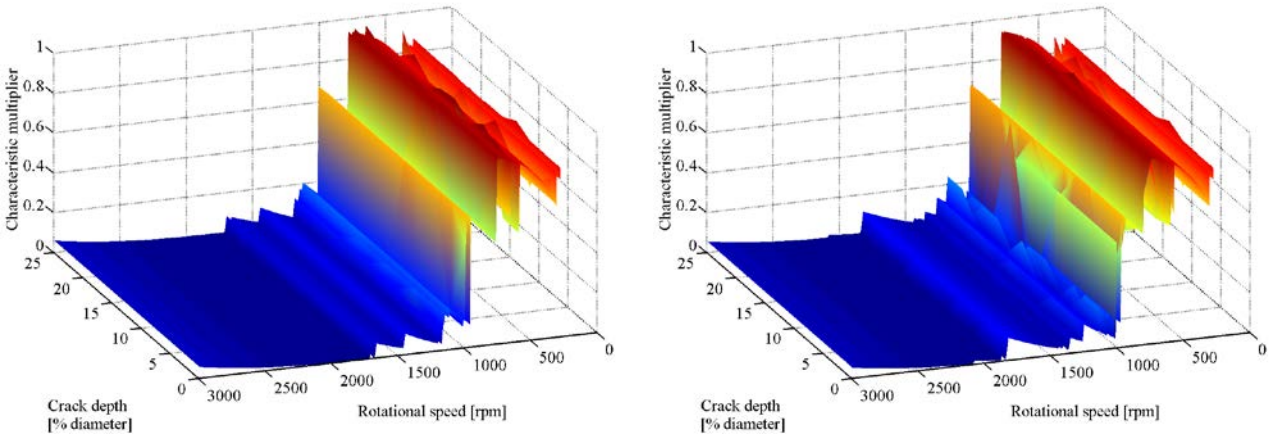


**Figure 11. First characteristic multiplier for a crack in the 10$^{th}$ element.**

As previously stated, with the aim of assessing the dependence of the stability on the crack position, simulations for a crack in the 18$^{th}$ element of the generator have also been performed. The distributions of the first characteristic multiplier for the four modelling configurations and for this crack position are shown in figure 12. Similar to the results obtained for a crack in the 10$^{th}$ element, the stability threshold is not reached for any combination of rotational speeds and crack depths considered.

*Configuration 1*

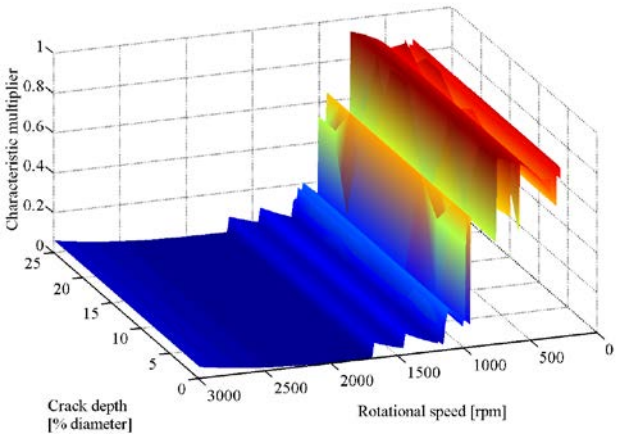


*Configuration 2*

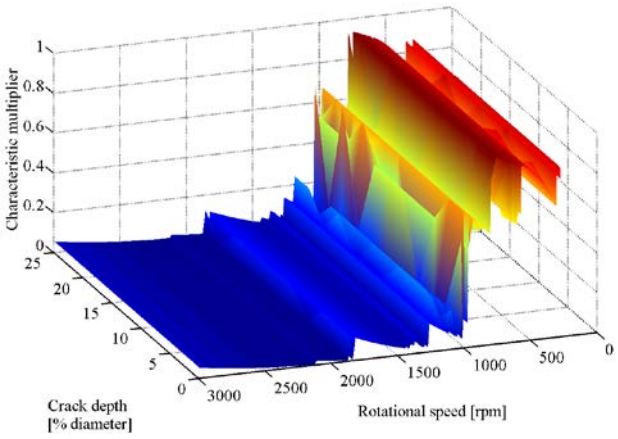


*Configuration 3*

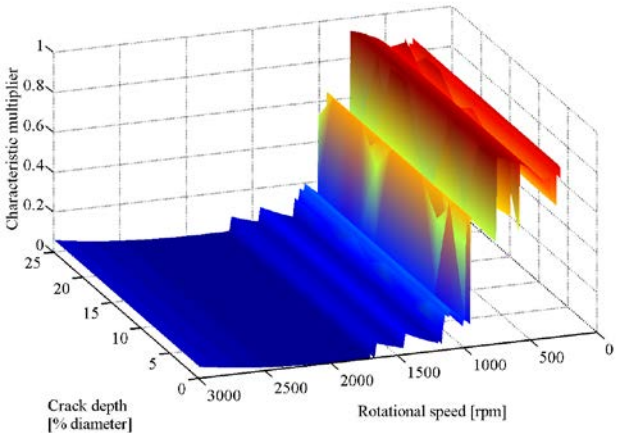


*Configuration 4*

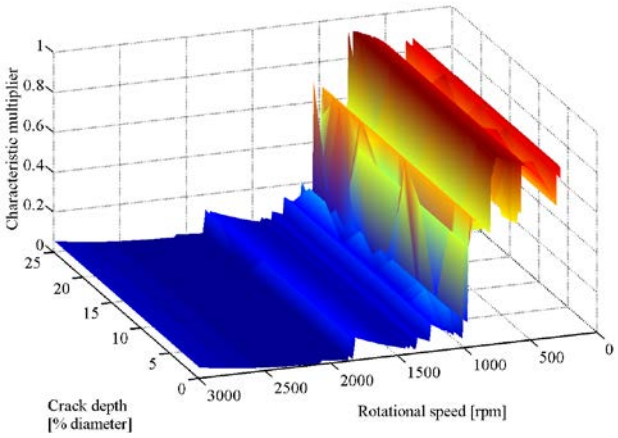


**Figure 12. First characteristic multiplier for a crack in the 18$^{th}$ element.**

The distributions of the first characteristic multiplier, calculated for a crack in the final part of the rotor (i.e., the 23$^{rd}$ element of the generator) and for different modelling configurations, are shown in figure 13. For this crack position, the generator behaviour is also stable regardless of the rotational speed and the crack depth. Moreover, the obtained trends are quite similar to those characterising the other crack positions: independent of the configuration, high multiplier values are reached for low rotational speeds, while the multiplier remains close to zero at high speeds.

*Configuration 1* *Configuration 2*

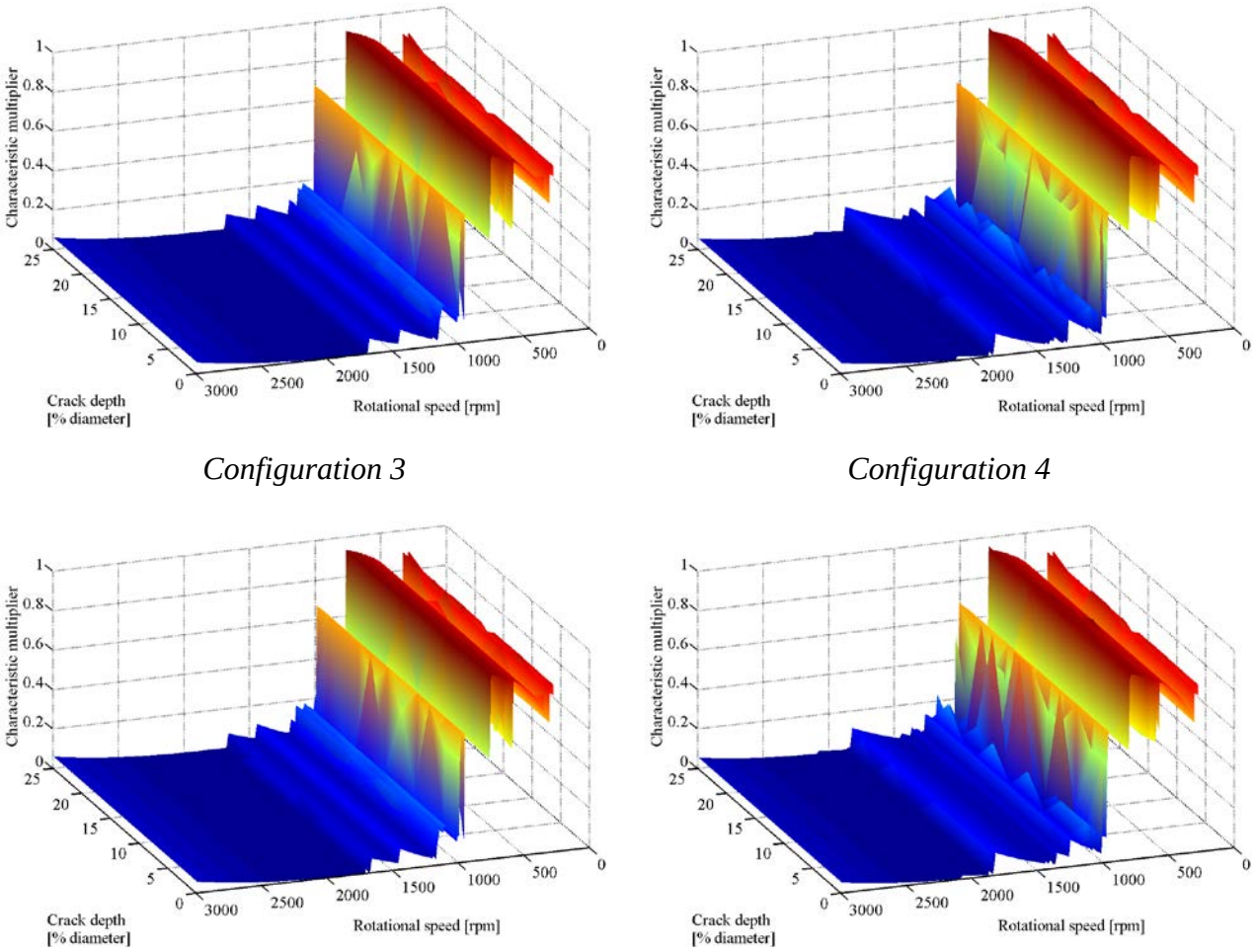


*Configuration 3* *Configuration 4*

**Figure 13. First characteristic multiplier for a crack in the 23rd element.**

Next, another group of multipliers is considered, and the 40th characteristic multiplier is taken as an example. The corresponding distributions are shown in figure 14 for a crack located in the 10th element.

In contrast to the first multiplier (see figure 11), whose values were reduced with the increase in rotational speed, in this case, the high values characterising low speeds decayed at 1200 rpm and increased again for higher rotational speeds. This result notwithstanding, the conclusion of the FA is the same: the dynamic behaviour of the generator is stable over the entire rotational speed-crack depth plane because the 40th characteristic multiplier does not exceed the value of one for all four configurations.

*Configuration 1*

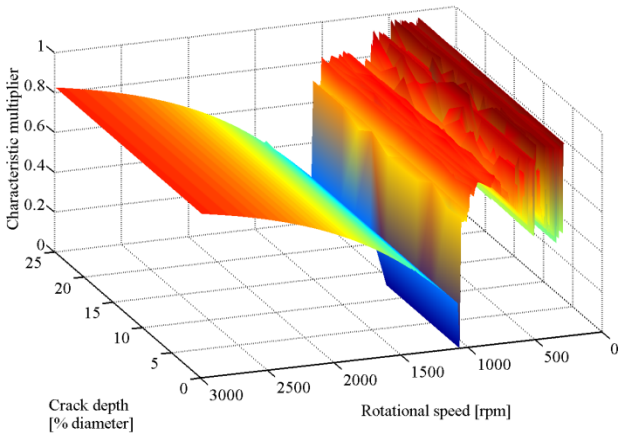


*Configuration 2*

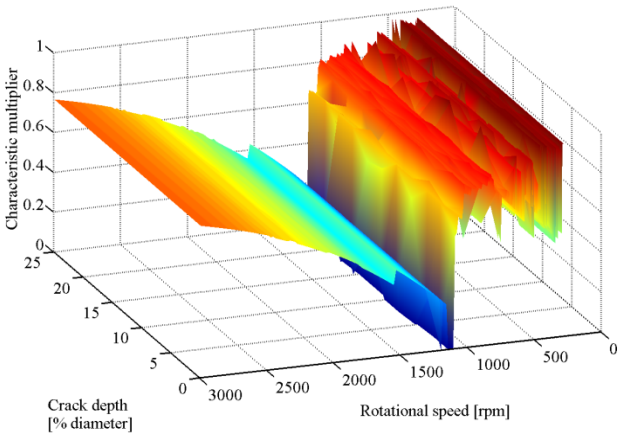


*Configuration 3*

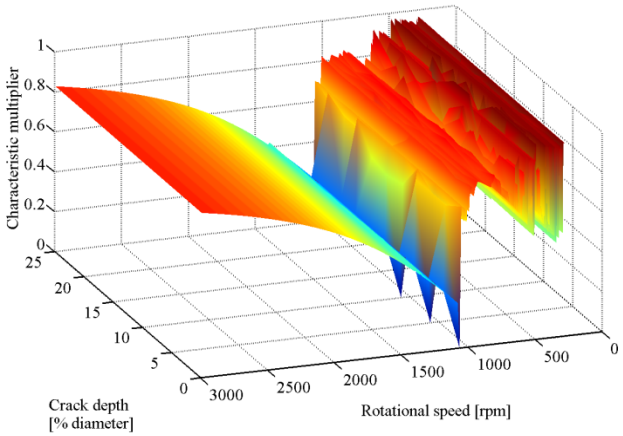


*Configuration 4*

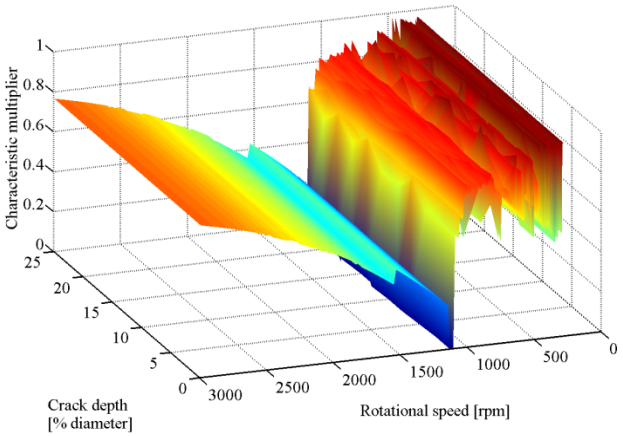


**Figure 14. 40$^{th}$ characteristic multiplier for a crack in the 10$^{th}$ element.**

*Configuration 1*

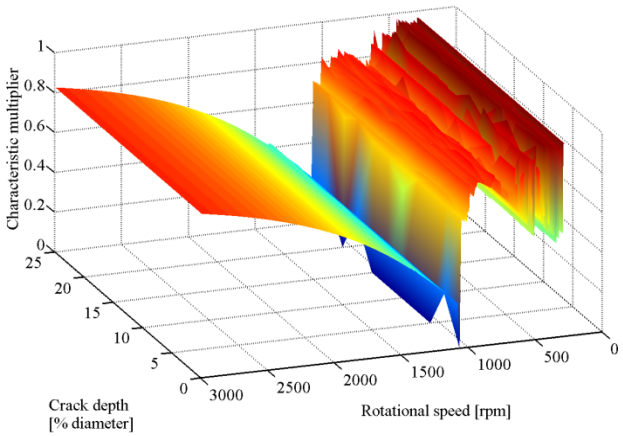


*Configuration 2*

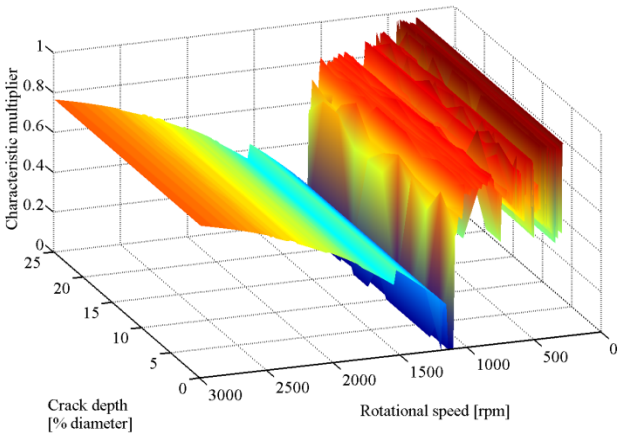


*Configuration 3*

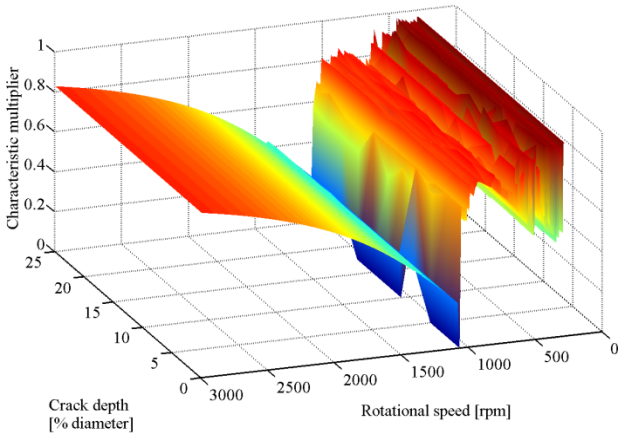


*Configuration 4*

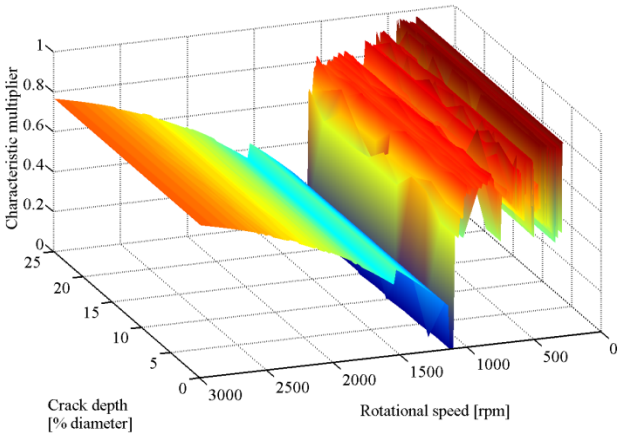


**Figure 15. 40$^{th}$ characteristic multiplier for a crack in the 18$^{th}$ element.**

*Configuration 1* *Configuration 2*

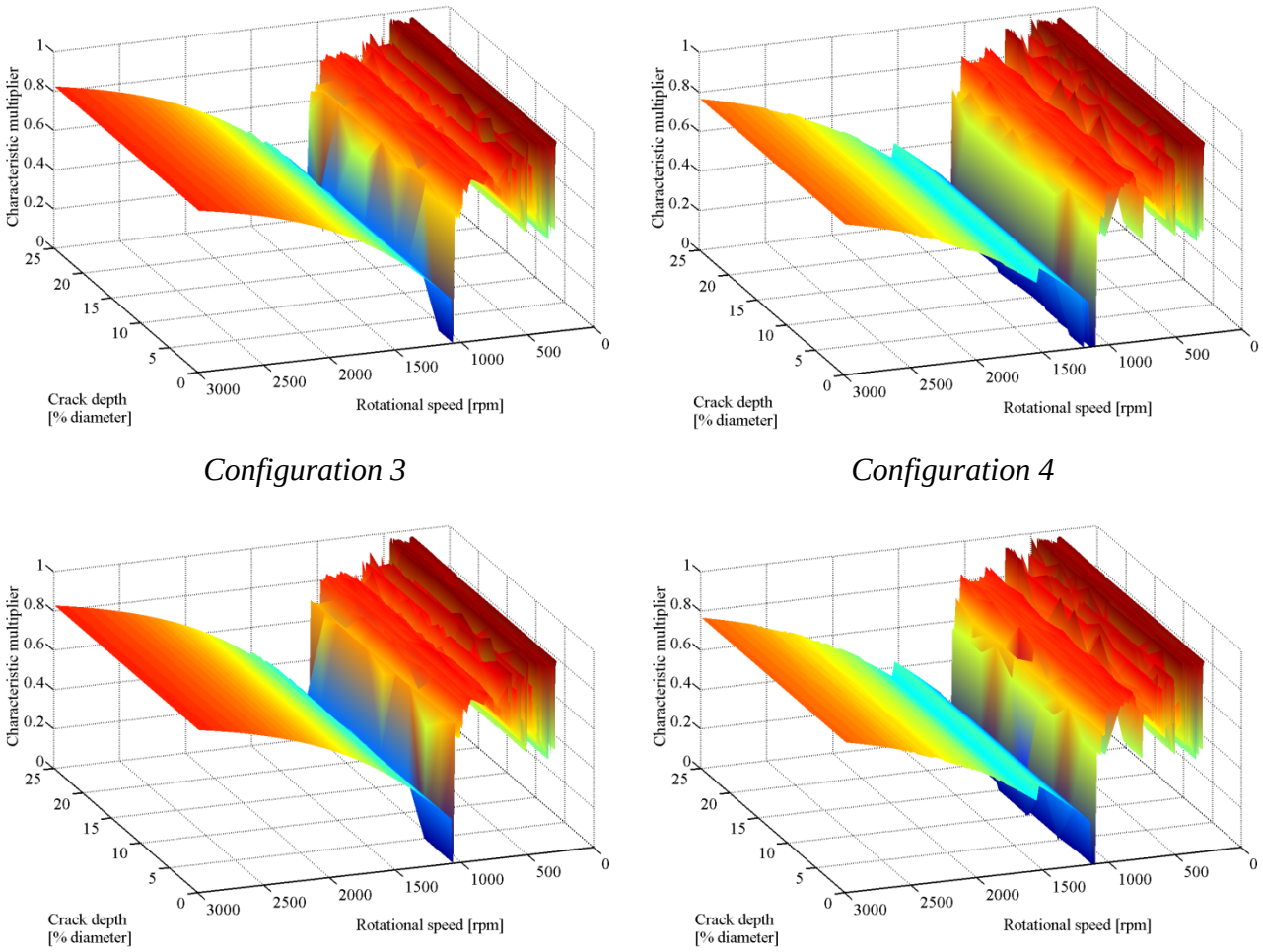


*Configuration 3* *Configuration 4*

**Figure 16. 40th characteristic multiplier for a crack in the 23rd element.**

Similar results are also obtained for cracks located in the 18th and 23rd elements of the generator, as shown respectively in figure 15 and figure 16.

For the sake of brevity, no further distributions of multipliers are reported, but none reach the instability threshold in the considered ranges of rotational speed and crack depth.

This result implies that the generator under consideration never reaches instability, even with a rather deep crack located in the positions where it frequently develops in practice. These theoretical results are confirmed by the experimental evidence from the corresponding real machines (similar generators) described in [1][16][17].

The differences in behaviour between a cracked Jeffcott rotor and the model of a cracked real machine rotor can be explained by considering that the stability of the system is determined by the structure of its matrices. The anisotropic and periodical components caused by the crack in the stiffness matrix are less influential in a system with several d.o.f.s, where few elements of the stiffness matrix are involved, than in a Jeffcott rotor.

In other words, the crack effect is “local” for any model of a real machine and “global” for any Jeffcott rotor. Moreover, any machine equipped with journal bearings contains high damping that may significantly raise the instability threshold.

However, the results obtained in this paper are rather remarkable because they show that in systems that are more realistic than the Jeffcott rotor model, the instability onset does not occur even in the presence of cracks with a depth that is considered dangerous for machine operation.

This result implies that the commonly acknowledged symptoms used to diagnose the presence of a transverse crack (see the details reported in [1]) are the most suitable. The instability might not occur in real rotors in practice before that crack has propagated to the extent that the machine operation would be impossible.

## 7. Conclusions

One of the most studied faults in rotating machines is that of the transverse crack, and it is commonly acknowledged in the literature that cracks in a horizontal rotating shaft can cause instability of the rotor dynamic behaviour. This consideration follows from the application of Floquet theory to a hinge model on a Jeffcott rotor.

The aim of the paper is the application of Floquet analysis to a real rotor model to study the stability of the shaft in the presence of a transverse crack. Certain important modifications have been introduced by the authors via the algorithms presented in the literature for the purpose of performing multi-dimensional Floquet analysis. These improvements have allowed this method to be suitable for models characterised by a high number of d.o.f.s.

Multi-dimensional Floquet analysis has been performed on a model of a generator that also considers the journal bearings and foundations, and different modelling configurations and crack positions have been considered to assess their effects on the rotor stability. Additionally, an improved algorithm has been developed by the authors and introduced in this work to perform multi-dimensional Floquet analysis in an acceptable time. The simulations have provided significant results: for any rotational speed in the machine operating range, crack depth, crack position and modelling of bearings and foundation, the rotor can be characterised by stable behaviour. All of the characteristic multipliers calculated for all of the considered configurations have assumed values less than one.

Considering the results provided by the Floquet analysis, it is possible to state that instability does not arise in this case. This rotor behaviour is consistent with case histories reported in the literature of generators affected by deep cracks, as listed in the paper. Obviously, the results obtained by the present Floquet analysis cannot be assumed as valid for all rotating machines affected by transversal cracks. However, the result obtained with the proposed version of the Floquet analysis represents a remarkable and original achievement.

It is authors' opinion that the instability, which results from Floquet analysis on hinge models with a Jeffcott rotor, is mainly due to the large effects of the stiffness variation on the global dynamic behaviour of the Jeffcott rotor model. By considering a complex model of a real industrial rotor, the stiffness variation associated with the crack becomes a "local" effect, as it is in practice.

## References


[1] Bachschmid N., Pennacchi P., Tanzi E. (2010) Cracked Rotors, A Survey on Static and Dynamic Behaviour Including Modelling and Diagnosis, Springer, Berlin – Heidelberg, ISBN 978-3-642-01484-0 (Print) 978-3-642-01485-7 (Online), 1-401.

[2] Ishida Y. (2008) Cracked Rotors: Industrial Machine Case Histories and Nonlinear Effects Shown by Simple Jeffcott Rotor. Mechanical Systems and Signal Processing, 22(4), 805-817, Special Issue: Crack Effects in Rotordynamics, N. Bachschmid and P. Pennacchi guest editors.

[3] Gasch R. (1976) Dynamic behaviour of a simple rotor with a cross-sectional crack. Conference on Vibrations in Rotating Machinery, IMechE, London, 1976, 123-128.

[4] Gasch R. (1993) A survey of the dynamic behaviour of a simple rotating shaft with transverse crack. Journal of sound and vibration, 160(2), 313-332.
[5] Meng G., Gasch R. (2000) Stability and Stability Degree of a Cracked Flexible Rotor Supported on Journal Bearings. Journal of Vibration and Acoustics, 122(2) April 2000, 116-125.
[6] Gasch R. (2008) Dynamic behaviour of the Laval rotor with a transverse crack. Mechanical Systems and Signal Processing, 22(4) (2008), 790-804, Special Issue: Crack Effects in Rotordynamics, N. Bachschmid and P. Pennacchi guest editors.
[7] Muszyńska A. (1985) Demonstration of various rotor instabilities (exhibit of Bently rotor dynamics research corporation laboratory rigs at symposium on instability in rotating machinery). NASA Conference Publication, 409-413.
[8] Huang S. C., Huang Y.M., Shish S.M. (1993) Vibration and stability of a rotating shaft containing a transverse crack. Journal of Sound and Vibration, 162(3), 387-401.
[9] Sekhar A.S. (1999) Vibration characteristics of a cracked rotor with two open cracks. Journal of Sound and Vibration, 223(4), 497-512.
[10] Sekhar A.S., Kumar Dey J. (2000) Effects of cracks on rotor system instability. Mechanism and Machine Theory, 35(12), 1657-1674.
[11] Yang B., Suh C.S., Chan A.K. (2002) Characterization and detection of crack-induced rotary instability Journal of Vibration and Acoustics, Transactions of the ASME, 124(1), 40-48.
[12] Zhu C., Robb D.A., Ewins D.J. (2003) The dynamics of a cracked rotor with an active magnetic bearing. Journal of Sound and Vibration, 265(3), 469-487.
[13] Lin F.-S., Meng G., Hahn E. (2004) Nonlinear dynamics of a cracked rotor in a manoeuvring aircraft. Applied Mathematics and Mechanics (English Edition), 25(10), 1139-1150.
[14] Chen C., Dai L., Fu Y.(2007) Nonlinear response and dynamic stability of a cracked rotor. Communications in Nonlinear Science and Numerical Simulation, 12(6), 1023-1037.
[15] Sinou J.J. (2007) Effects of a crack on the stability of a non-linear rotor system. International Journal of Non-Linear Mechanics, 42(7), 959-972.
[16] Lapini G.L., Zippo M., Bachschmid N., Collina A., Vallini A. (1993) Experimental tests and model based calculations for the diagnosis of a crack in a 320 MW generator. Diagnostics of rotating machines in power plants, CISM/IFToMM Symposium Proceedings, Udine, Italy, 87-97.
[17] Bicego V., Lucon E., Rinaldi C., Crudeli R. (1999) Failure analysis of a generator rotor with a deep crack detected during operation: Fractographic and fracture mechanics approach. Nuclear Engineering and Design, 188(2), 173-183.
[18] Schabtach C., Fogleman E.L., Rankin A.W., Winne D.H. (1956) Report of the Investigation of Two Generator Rotor Fractures. Transactions of the ASME, 78(10), 1567.
[19] Nilsson L.R.K. (1982) On the Vibration Behaviour of a Cracked Rotor. IFToMM International Conference on Rotordynamic Problems in Power Plants, Rome, Italy, 515-524.
[20] Sanderson A.F.P. (1992) The Vibration Behaviour of a Large Steam Turbine Generator During Crack Propagation Through the Generator Rotor. IMechE International Conference on Vibrations in Rotating Machinery, Bath, UK, paper C432/102, 263-273.
[21] Schöllhorn K., Ebi G., Steigleder K. (1993) Frettinganrisse in einem 936-MW Turbogeneratorrotor. VGB Kraftwerkstechnik, 73(4), 340-344.
[22] Mayes I.W., Davies W.G.R. (1976) The vibrational behaviour of a rotating shaft system containing a transverse crack Paper C 168/76, in: International Mechanical Engineering Conference Vibration in Rotating Machinery, Cambridge, UK, 1976.

[23] Papadopoulos C.A. (2008) The strain energy release approach for modeling cracks in rotors: A state of the art review. Mechanical Systems and Signal Processing, 22(4), 763-789. Special Issue: Crack Effects in Rotordynamics, N. Bachschmid and P. Pennacchi guest editors.
[24] Darpe A.K., Gupta K., Chawla A. (2004) Coupled bending, longitudinal and torsional vibrations of a cracked rotor, Journal of Sound and Vibration 269 (1–2) (2004), 33–60.
[25] Papadopoulos C.A. (2004) Some comments on the calculation of the local flexibility of cracked shafts, Journal of Sound and Vibration 278 (4–5) (2004), 1205–1211.
[26] Wu X., Friswell M.I., Sawicki J.T., Baaklini G.Y. (2005) Finite element analysis of coupled lateral and torsional vibrations of a rotor with multiple cracks, in: Proceedings of ASME Turbo Expo 2005 Gas Turbine Technology: Focus for the Future, Reno (NV), Jun 6–9, vol. 4, 2005, 841–850.
[27] Varé C., Andrieux S. (2005) Modeling of a cracked beam section under bending, SMIRT 18, in: 18th International Conference on Structural Mechanics in Reactor Technology, Beijing, China, 7–12 August 2005, 2005, pp. 281–290.
[28] Georgantzinos S.K., Anifantis N.K. (2008) An insight into the breathing mechanism of a crack in a rotating shaft. Journal of Sound and Vibration, 318(1-2), 279-295.
[29] Bachschmid N., Pennacchi P., Tanzi E.(2008) Some remarks on breathing mechanism, on non-linear effects and on slant and helicoidal cracks. Mechanical Systems and Signal Processing, 22(4), 879-904. Special Issue: Crack Effects in Rotordynamics, N. Bachschmid and P. Pennacchi guest editors.
[30] Bachschmid N., Tanzi E. (2003) Stresses and Strains in Correspondence of a Transverse Crack in a Shaft: Effect of Crack Closure. Crack Path CP 2003 Int. Conference, September 2003, Parma, Italy.
[31] Moore G. (2005) Floquet theory as a computational tool, SIAM Journal on Numerical Analysis, 42(6), 2522-2568.
[32] Jordan D.W., Smith P., Nonlinear ordinary differential equation. An introduction to dynamical system, Third Edition, Oxford University Press Inc., New York.
[33] Friedmann P.P. (1990) Numerical methods for the treatment of periodic system with applications to structural dynamics and helicopter rotor dynamics. Computer & Structures, 35(4), 329-347.
[34] Sinha S.C., Wu D.H. (1990) An efficient computational scheme for analysis of periodic systems. Journal of Sound and Vibration, 151(1), 91-117.
[35] Khasawneh F.A., Mann B.P., Butcher E.A. (2011) A multi-interval Chebyshev collocation approach for the stability of periodic delay systems with discontinuities. Communications in Nonlinear Sciences and Numerical Simulation, 16, 4408-4421.
[36] Bayly P.V., Halley J.E., Mann B.P., Davies M.A. (2001) Stability of Interrupted Cutting by Temporal Finite Element Analysis. Proceedings of the ASME 2001 Design Engineering Technical Conferences, Pittsburgh, Pennsylvania, paper no. DETC2001/VIB-21581.
[37] Insperger T., Mann B.P., Stépán G., Bayly P.V. (2003) Stability of Up-Milling and Down-Milling, Part 1: Alternative Analytical Methods. International Journal of Machine Tools & Manufacture, 43(1), 25-34.
[38] Insperger T., Stépán G. (2004) Vibration Frequencies in High-Speed Milling Processes or a Positive Answer to Davies, Pratt, Dutterer and Burns. Journal of Manufacturing Science and Engineering, 126(3), 481-487.
[39] Moler C., Van Loan C, (1978), Nineteen ways to compute the exponential of a matrix, SIAM Review, 20(4), 801-836.

[40] Van Loan C., (1977), The Sensitivity of the Matrix Exponential, SIAM Journal on Numerical Analysis, 14(6), 971-981.
[41] Moler C., Van Loan C., (2003), Nineteen dubious ways to compute the exponential of a matrix, twenty-five years later, SIAM Review, 45(1), 3-49.
[42] Bickart T. A., (1968), Matrix exponential: Approximation by truncated power series, Proceedings of the IEEE, 56, 872-873.
[43] Liou M. L., A novel method of evaluating transient response, Proceedings of the IEEE, 54 (1966), 20-23.
[44] Fair W. Luke Y. L., Pade approximations to the operator exponential, Numerische Mathematik 14 (1970), 379-382.
[45] Ward R. C., (1977), Numerical computation of the matrix exponential with accuracy estimate, SIAM Journal of Numerical Analysis, 14(4), 600–610.

**Figure captions**